Supporting Information

$[Cu_{18}H_3(S\text{-}Adm)_{12}(PPh_3)_4Cl_2]$: fusion of Platonic and Johnson solids through a Cu(0) center and its photophysical properties

Anish Kumar Das,[a] Sourav Biswas,[a] Vaibhav S. Wani,[a] Akhil S. Nair,[b] Biswarup Pathak,[b] Sukhendu Mandal[a]*

[a]School of Chemistry, Indian Institute of Science Education and Research Thiruvananthapuram, Thiruvananthapuram, Kerala 69551, India. E-mail: sukhendu@iisertvm.ac.in

[b]Department of Chemistry, Indian Institute of Technology, Indore, Madhya Pradesh 453552, India.

Table of contents

Experimental

Materials

Tetrakis(acetonitrile)copper(I) tetrafluoroborate ($Cu(CH_3CN)_4BF_4$), triphenylphosphine (PPh_3), 1-adamantane thiol (Adm-SH), sodium borohydride ($NaBH_4$), tetra-n-butylammonium hexafluorophosphate ($TBAPF_6$), β-cyclodextrin were procured from Sigma-Aldrich. HPLC grade solvents- chloroform, dichloromethane, acetonitrile, methanol, and n-hexane were purchased from Spectrochem. Milli-Q water was utilized throughout the experiments.

Synthesis of Cu_{18} NC

Initially, 50 mg of $Cu(CH_3CN)_4BF_4$ and 50 mg of PPh_3 were dissolved in the mixture solution of 2 mL acetonitrile and 0.5 mL chloroform at room temperature. After 5 min of stirring, 20 mg of Adm-SH was added to the reaction mixture and continued stirring. After the addition of 50 mg $NaBH_4$ dissolved in 2.5 mL methanol, the color of the solution becomes red from colorless. The reaction was kept for another 1 h under continuous stirring. After completion, the reaction mixture was centrifuged and collected the red precipitate. After drying properly, the precipitate was dissolved in the solvent mixture of chloroform/hexane (volume ratio 1:1). The final clear solution was kept for crystallization at ambient conditions. After 7 days, red-colored cubic crystals were obtained.

The synthesis of atomically precise Cu NCs is much more challenging compared to the Ag NCs and Au NCs due to the low reduction potential and the high reactivity of the Cu with respect to Ag and Au. Hence, the synthesis of Cu NCs containing zero-valent Cu atoms in the core experiences more complications. In the synthesis of reported $[Cu_{32}(PET)_{24}H_8Cl_2][PPh_4]_2$, it had been shown that tetramethylethylenediamine was an important reagent for the synthesis where in the first step Cu(I) complex was formed, followed by the reduction of the complex was occurred under Ar atmosphere, though the tetramethylethylenediamine is not attached in the final product.[S1] Doubly charged Cu_{32} NCs stabilized by PPh_4^+ were formed where no Cu(0) is present. In the synthesis of $[Cu_{25}H_{10}(SPhCl_2)_{18}]^{3-}$, Cu(II) salt was used as a precursor and after reduction by $NaBH_4$, ended up with the anionic NCs with again all Cu is in +1 state.[S2] In both cases, the single crystals were obtained at low temperatures. In the synthesis of reported $[Cu_{61}(S^tBu)_{26}S_6Cl_6H_{14}]^+$, a mild

reducing agent borane tert-butylamine complex was used instead of the strong reducing agent $NaBH_4$ to make the largest Cu(0)-containing core-shell copper NCs.[S3] In the synthesis of $[Cu_{15}(PPh_3)_6(PET)_{13}]^{2+}$, $[Cu_{36}H_{10}(PET)_{24}(PPh_3)_6Cl_2]$, and $[Cu_{81}(PhS)_{46}(^tBuNH_2)_{10}(H)_{32}]^{3+}$, a one-pot direct reduction strategy had been followed.[S4, S5, S6] In the case of Cu_{15} NC and Cu_{36} NC, $NaBH_4$ was used and in the case of Cu_{81} NC, $^tBuNH_2{\cdot}BH_3$ was used as reducing agents, though in all cases, Cu(I) salts were taken as a metal precursor. It has been observed that in the case of the mild reducing agent which gives rise to high-nuclearity Cu NC compared to the strong reducing agent under ambient conditions. In both cases, there is no Cu(0) atom. But in this work, Cu_{18} NC was synthesized by a facile one-pot synthetic strategy. This synthetic procedure is almost the same as the procedure of Cu_{36} NC. Only we have changed the PET ligand with the bulky adamantane thiol ligand in our synthesis and that bulkiness of the ligand may induce the stability of the Cu(0) atom at the center of the Cu_{10} core.

Synthesis of Cu_{18}D NC

The same procedure was adopted whatever was mentioned for the synthesis of the Cu_{18} NC. Instead of $NaBH_4$, we have used $NaBD_4$ as a reducing agent.

Synthesis of $Cu_{18} \cap$ β-CD_1

Initially, 3 mg of Cu_{18} NC was dissolved in 5 mL of tetrahydrofuran and then a 2 mL aqueous solution of β-CD (2 mg/mL) was added. The resultant reaction mixture was then sonicated for 15 min and kept for stirring for 1 h with a recurrent sonication for 2 min at every 15 min intervals. The obtained solution was washed several times with water. Finally, the aqueous phase was removed and the organic phase was dried.

X-ray Crystallography details

Single-crystal data of Cu_{18} NC was collected on a Rigaku Oxford Diffraction XtaLAB Synergy-S diffractometer equipped with a HyPix-6000HE Hybrid Photon Counting (HPC) detector operating in shutter less mode and an Oxford Cryosystems Cryostream 800 Plus at 173 K using Cu Kα (λ = 1.54184 Å) from PhotonJet micro-focus X-ray Source. Data were processed using the *CrystAlis*^{Pro} software suite.[S7] The structure was solved using the charge-flipping algorithm, as implemented in the program SUPERFLIP [S8] and refined by full-matrix

least-squares techniques against Fo^2 using the SHELXL program[S9] through the OLEX2 interface.[S10]

Computational details

The DFT calculations were done using Gaussian 09 D.01 program. [S11] B3LYP functional with Pople's 6–31G* basis set[S12, S13] was used for non-metal elements, and LANL2DZ-ECP (effective core potential) [S14, S15] was employed for Cu atoms, respectively. Chloroform solvent was considered to simulate the experimental non-polar solvent scenario. The TD-DFT calculations considered 300 singlet-to-singlet excitation energies. The -PPh_3 ligand is simplified to -PMe_3 during the calculation. Kohn-Sham orbital analysis has been performed for identifying the orbital contribution in molecular orbitals and corresponding energies by using the multi wave function 3.6 program.[S16, S17] The NMR spectrum is simulated by using the GIAO method implemented in Gaussian 09 D.01 program. [S18]

The projected density of states (PDOS) calculation for the compounds at the bulk level is carried out using Vienna Ab-Initio Simulation Package (VASP) by using Generalized gradient approximation of Perdew–Burke–Ernzerhof (PBE) functional.[S19, S20] Projector augmented wave (PAW) method is used for treating ion-electron interactions.[S21] The ionic relaxations have been carried out using a Conjugate gradient algorithm with convergence criteria of 10^{-4} eV for minimum energy and 0.05 eV $Å^{-1}$ for Hellmann-Feynman forces on atoms. Due to the large size of the unit cells of the compounds, the Brillouin zone was sampled at the Gamma point (1×1×1). For the PDOS calculation, a higher (2×2×2) K-point is used. The atomic charges are calculated using Bader charge analysis. [S22]

Instrumentation

A SHIMADZU UV-3800 spectrometer was used for measuring the absorbance spectra. Emission measurements were performed using a Fluorolog-3 spectrofluorimeter from Horiba Jobin Yvon. The relative quantum yield was determined by the best match of the excitation wavelength of a well-known chromophore such as pyrene with the NC and the excitation was fixed at 317 nm. The concentration of the chloroform solutions was fixed by adjusting the absorption 0.05 OD and measured the quantum yield at room temperature. A picosecond time-correlated single photon counting (TCSPC) system (Horiba Jobin Yvon-IBH) was utilized for

the measurement of emission lifetime. Transmission electron microscopy (TEM; FEI Tecnai G2 F30 S-Twin; 300 kV), scanning electron microscope (SEM), and energy-dispersive X-ray spectroscopy (EDS; FEI Nova NANOSEM 450) were used. X-ray photoelectron spectroscopy (XPS) and ultraviolet photoelectron spectroscopy (UPS) measurements have been done by using the Omicron Nanotech instrument (MgK_α radiation at 1253.6 eV). All binding energies were referenced to the neutral C 1s peak at 284.8 eV. The thermo-gravimetric analysis (TGA) was done on SDT Q600 (Shimadzu) instrument with a heating rate of 10 $^oC\ min^{-1}$ under N_2 atmosphere. Cyclic Voltammogram was done by using a CH instrument with a three-electrode system where glassy carbon was used as a working electrode, graphite electrode served as a counter electrode and silver wire was used as a reference electrode in dichloromethane solvent. In this organic solvent, 0.5 M $[(^nBu)_4N]PF_6$ salt was added as a supporting electrolyte. We have calibrated against the standard reference electrode (Ag/Ag^+). Bruker Avance III, 500 MHz, NMR was used for the ^1H and ^{31}P studies. Electron paramagnetic resonance (EPR) spectrum was recorded using MiniScope MS 5000 Magnettech EPR spectrometer. Waters Q-TOF mass spectrometer equipped with a Z-spray source was used for the electrospray ionization (ESI) mass spectrometry measurement in positive mode. Samples were dissolved in chloroform (1 mg/mL) and diluted by acetonitrile (1:1). The solution was infused at 20 µL/min. The spectrometer was operated in the mass range of m/z 1500–6000, capillary voltage was 2.9 kV, sampling cone 60, source temperature 70 °C source offset 28, desolvation temperature 100 °C, cone gas flow 20 L/Hr, desolvation gas flow 244 L/Hr. The chloroform solution of the synthesized NCs is drop-casted between the patterned gold electrodes deposited on the ceramic plate to form a thin layer of the material. The electrical and photoresponse measurements were observed using a Keithley 6712 electrometer using a laser of 360 nm wavelength and 10 mW.

The radiative and nonradiative rate constants calculation

The radiative rate (k_r) and nonradiative rate (k_{nr}) constants are calculated using the following equations

$$k_r = \frac{\phi}{\boldsymbol{\tau_{av}}} \quad \text{(S1)}$$

$$k_{nr} = \frac{(\mathbf{1}-\phi)}{\boldsymbol{\tau_{av}}} \quad \text{(S2)}$$

where, ϕ = Quantum yield; τ_{av} = Average emission lifetime.

Table S1. Crystal data and structure refinement parameters.

Identification code	**Cu_{18} NC**
CCDC number	2132516
Empirical formula	$C_{192}H_{242}Cl_2Cu_{18}P_4S_{12}$
Formula weight	4273.06
Temperature	173 (2) K
Wavelength	1.54184 Å
Crystal system	monoclinic
Space group	$P2_1/c$ (No. 14)
Unit cell dimensions	a = 19.2184 (2) Å; b = 47.4362 (6) Å, c = 24.0097 (3) Å; α = 90°; β = 100.5215 (12)°; γ = 90°
Volume	21520.4 (5) $Å^3$
Z	4
Density	1.319 mg/m^3
Absorption coefficient	3.783 mm^{-1}
F(000)	8808
Crystal size	0.15 × 0.06 × 0.04 mm^3
Theta range for data collection	2.517 to 67.079°
Limiting indices	-16<=h<=22, -56<=k<=56, -28<=l<=26
Reflections collected	136476
Independent reflections	37748 [R(int) = 0.0579]
Completeness to theta = 67.079°	98.3 %
Refinement method	Full-matrix least-squares on F^2
Data / restraints / parameters	37748 / 36 / 2065
Goodness-of-fit on F^2	1.016
Final R indices [I > 2sigma(I)]	R_1 = 0.0534, wR_2 = 0.1127
R indices (all data)	R_1 = 0.0722, wR_2 = 0.1199
Largest diff. peak and hole	1.307 and -0.629 e. $Å^{-3}$

Table S2. List of reported thiolate protected Cu NCs.

Sr. No.	Formula of Crystals	Presence of Cu(0)	Emission Property	Ref.
1	$[Cu_{15}(PPh_3)_6(SCH_2CH_2Ph)_{13}]^{2+}$	-	NIR emission	S4
2	$[Cu_{25}H_{10}(SPhCl_2)_{18}]^{3-}$	-	-	S2
3	$[Cu_{32}(SCH_2CH_2Ph)_{24}H_8Cl_2][PPh_4]_2$	-	-	S1
4	$[Cu_{36}H_{10}(SCH_2CH_2Ph)_{24}(PPh_3)_6Cl_2]$	-	-	S5
5	$[Cu_{61}(S^tBu)_{26}S_6Cl_6H_{14}]^+$	Partial Cu(0)	-	S3
6	$[Cu_{81}(PhS)_{46}(^tBuNH_2)_{10}(H)_{32}]^{3+}$	-	-	S6
7	$[Cu_{18}H_3(S\text{-}Adm)_{12}(PPh_3)_4Cl_2]$	One isolated Cu(0)	Violet emission	This work

Table S3. The obtained radiative, nonradiative rate constants, quantum yield and emission lifetime.

Compound	**Relative Quantum yield (ϕ)**	**Emission Lifetime (τ_{av}) (ns)**	**k_r (s^{-1})**	**k_{nr} (s^{-1})**
Cu_{18}	0.0032	0.26	1.23×10^7	3.83×10^9
$Cu_{18} \cap \beta\text{-}CD_1$	0.012	0.97	1.23×10^7	1.02×10^9

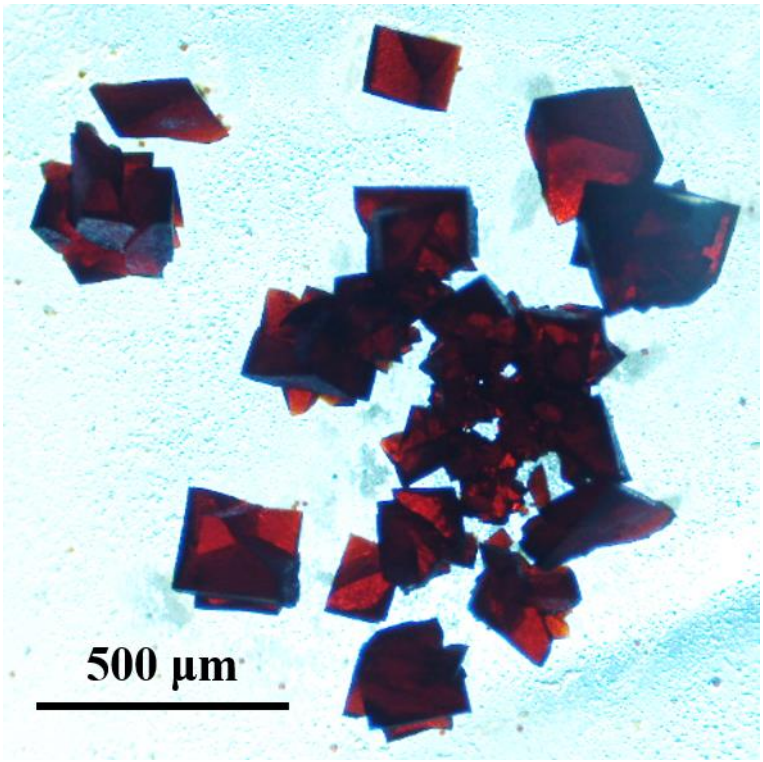

Fig. S1 The optical images of the Cu_{18} NC with cubic shape.

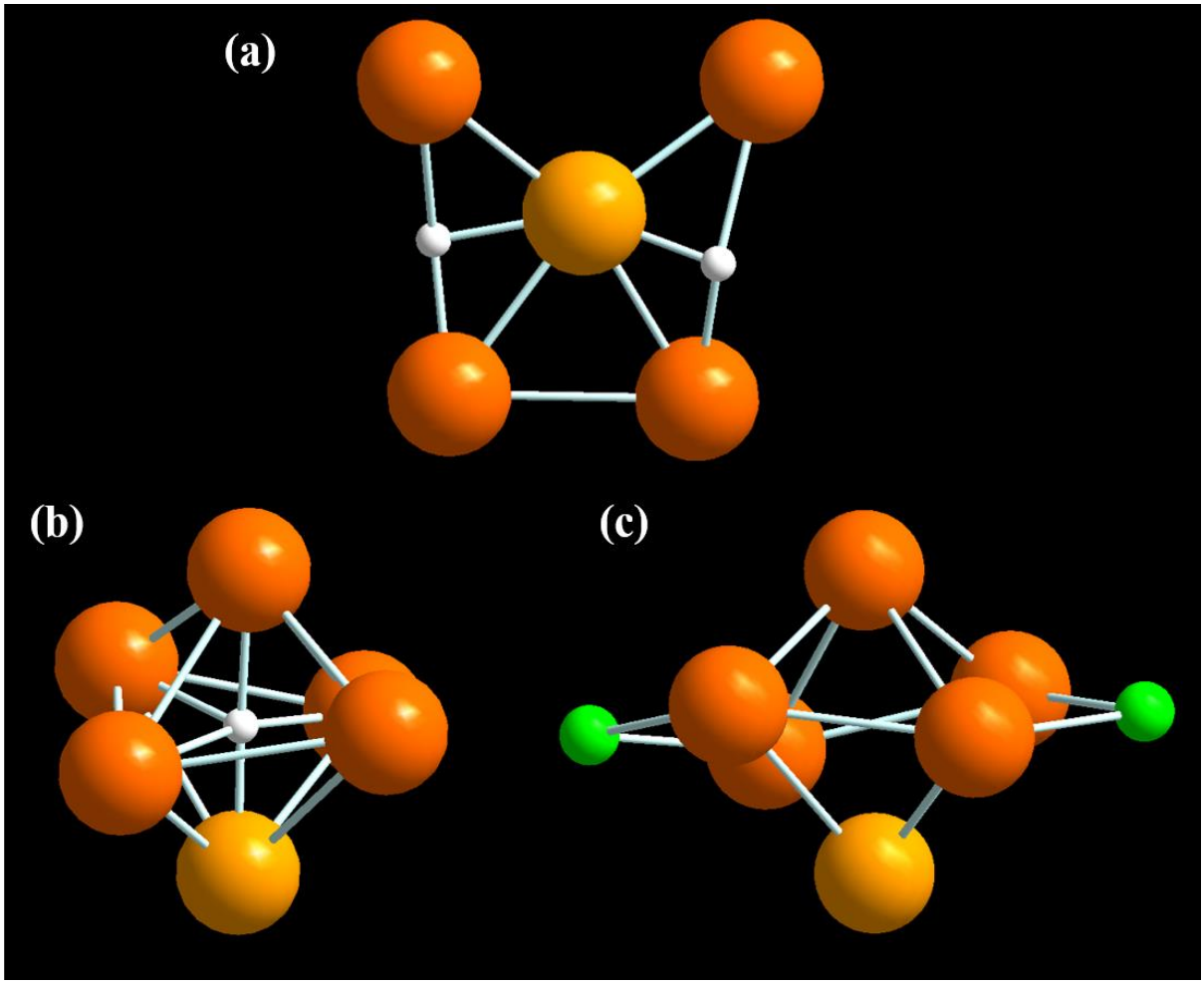

Fig. S2 (a) The attachment of two μ_3 bridged hydrides, and (b) one μ_5 bridged hydride with the core. (c) Attachment of two chloride atoms by μ_2 bridging mode at the two opposite positions of the square edges of the Cu_6 octahedron. Color legend; Cu, light and deep orange; Cl, green; H, white.

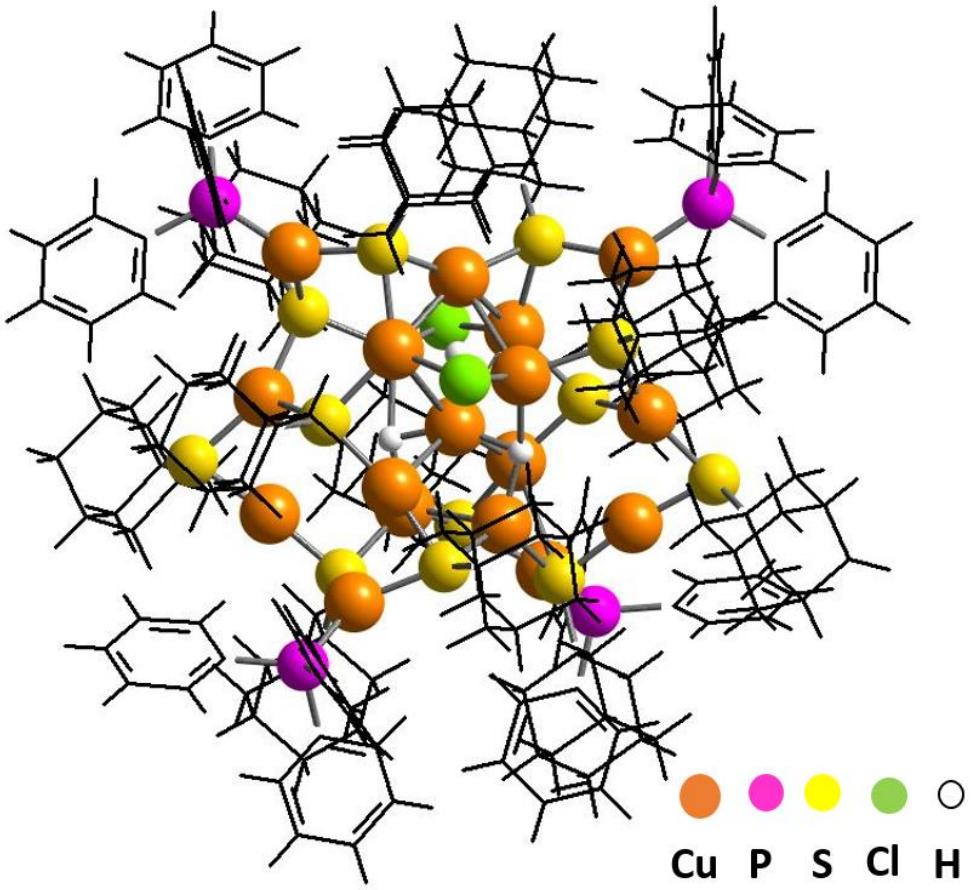

Fig. S3 DFT optimized structure of the Cu_{18} NC.

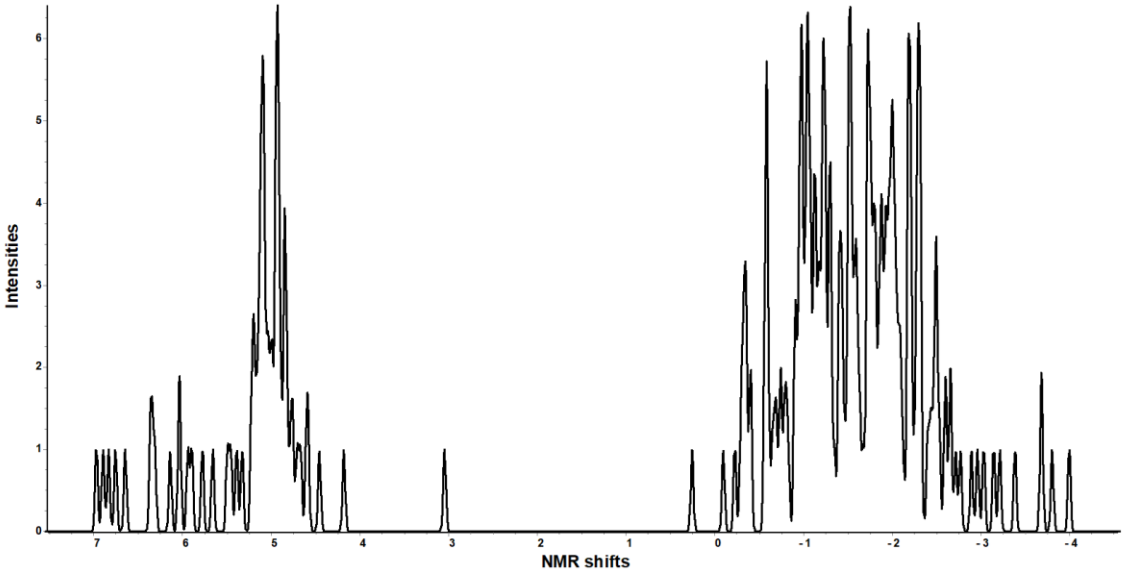

Fig. S4 GIAO ^{1}H NMR spectrum of the Cu_{18} NC.

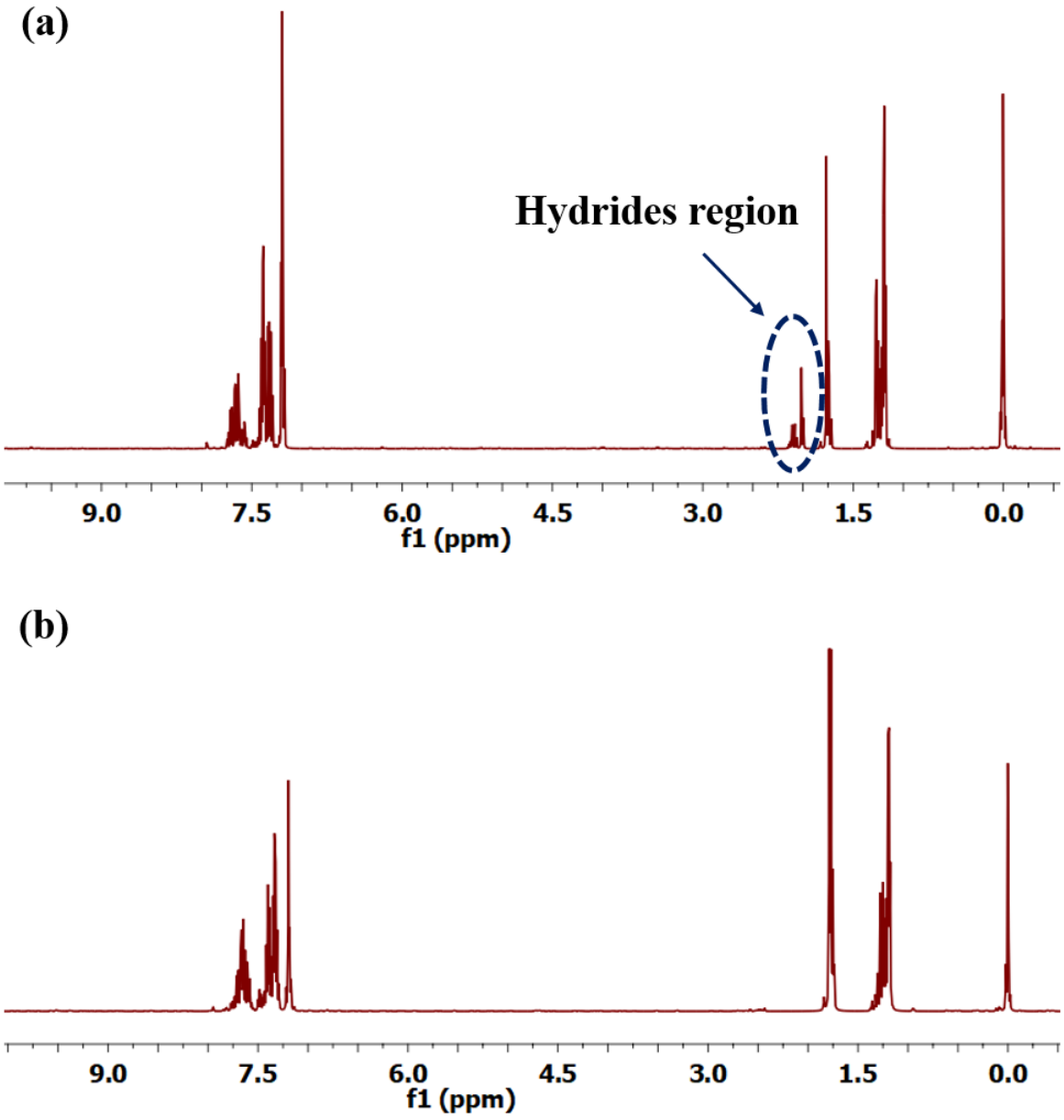

Fig. S5 ^{1}H NMR spectra in $CDCl_3$ of (a) Cu_{18} NC and (b) $Cu_{18}D$ NC.

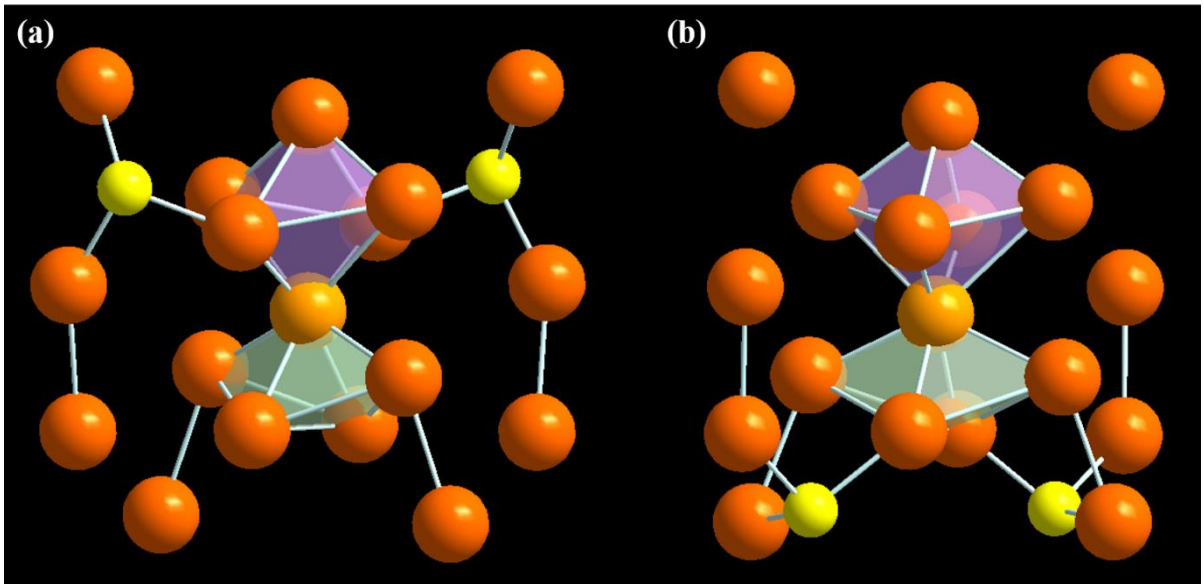

Fig. S6 μ_3 bridging mode of S (a) bonding between two Cu atoms of the motif and one Cu atom of the Cu_6 octahedron, and (b) bonding with two Cu atoms of the motif and one Cu atom of the Cu_5 distorted square pyramid. Color legend; Cu, light and deep orange; S, yellow.

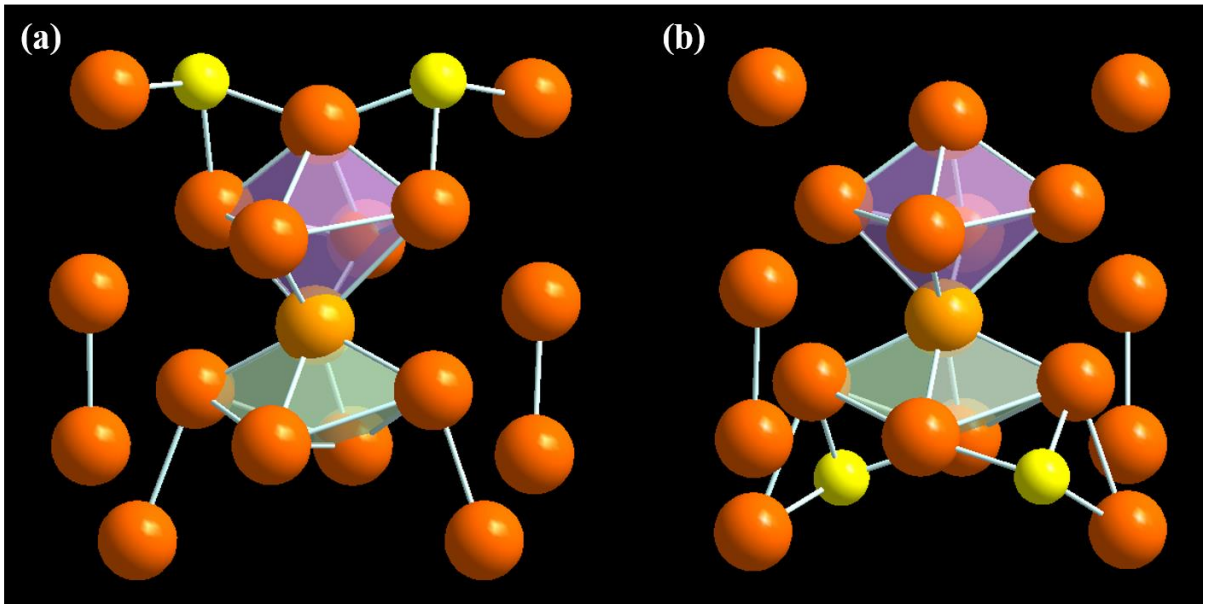

Fig. S7 μ_3 bridging mode of S (a) bonding between one Cu atom of the motif and two Cu atoms of the Cu_6 octahedron, and (b) bonding with one Cu atom of the motif and two Cu atoms of the Cu_5 distorted square pyramid. Color legend; Cu, light and deep orange; S, yellow.

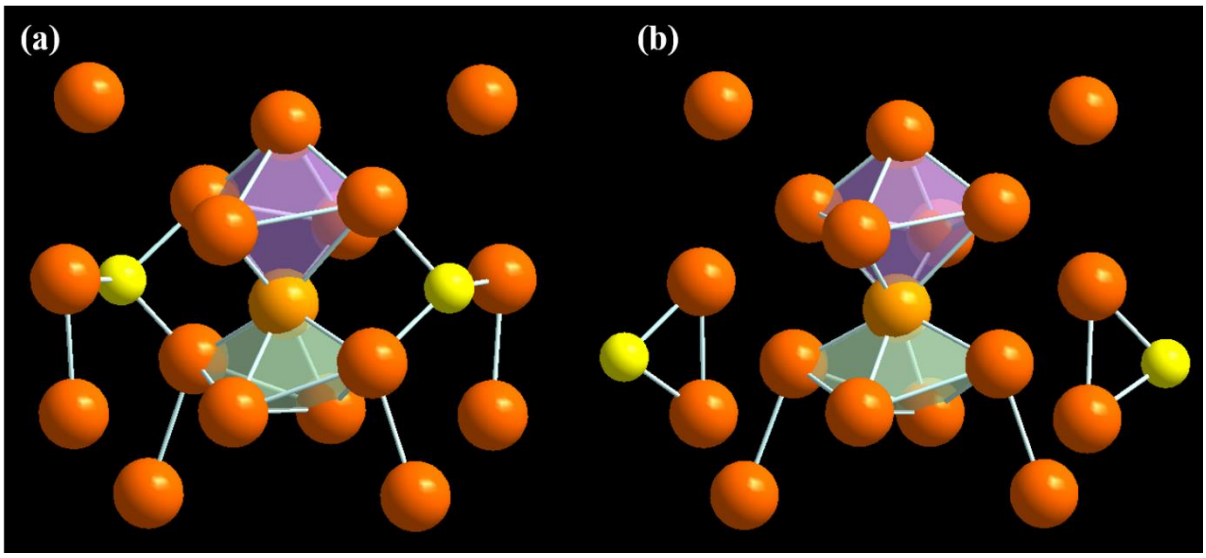

Fig. S8 (a) μ_3 bridging mode of S which are making connection among Cu_6 distorted octahedron, Cu_5 distorted square pyramid, and motif shell, and (b) μ_2 S atoms in the metal-ligand motifs. Color legend; Cu, light and deep orange; S, yellow.

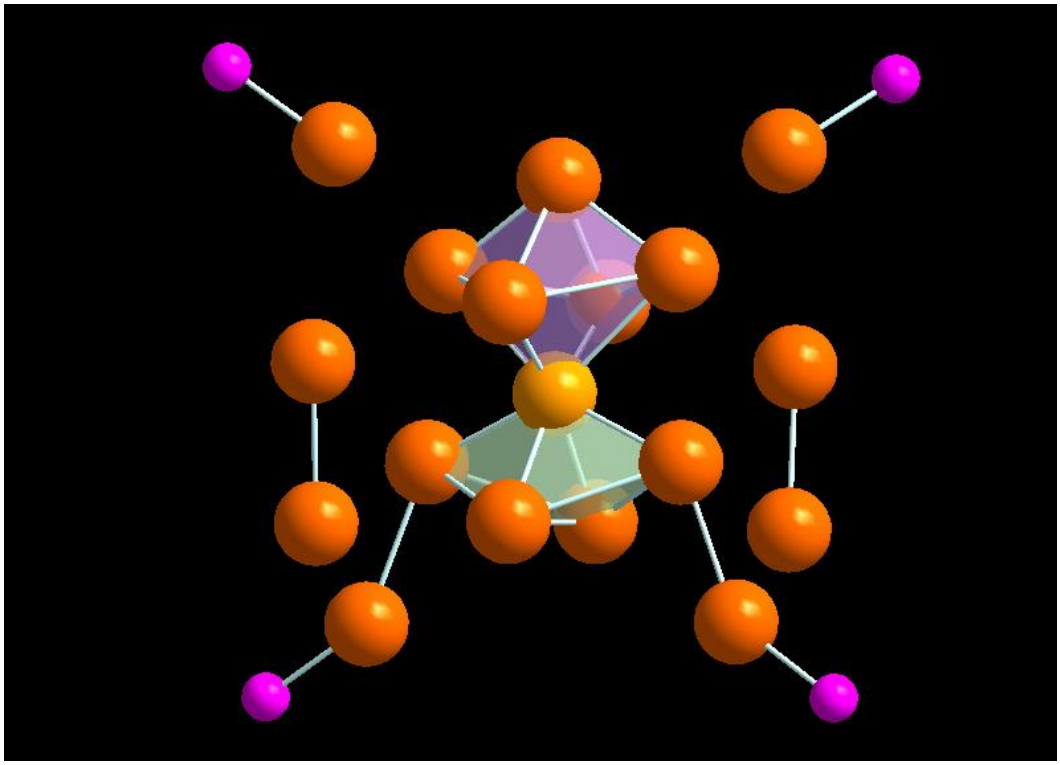

Fig. S9 Attachment of four P atoms with the four Cu atoms of the metal-ligand motifs. Color legend; Cu, light and deep orange; P, magenta.

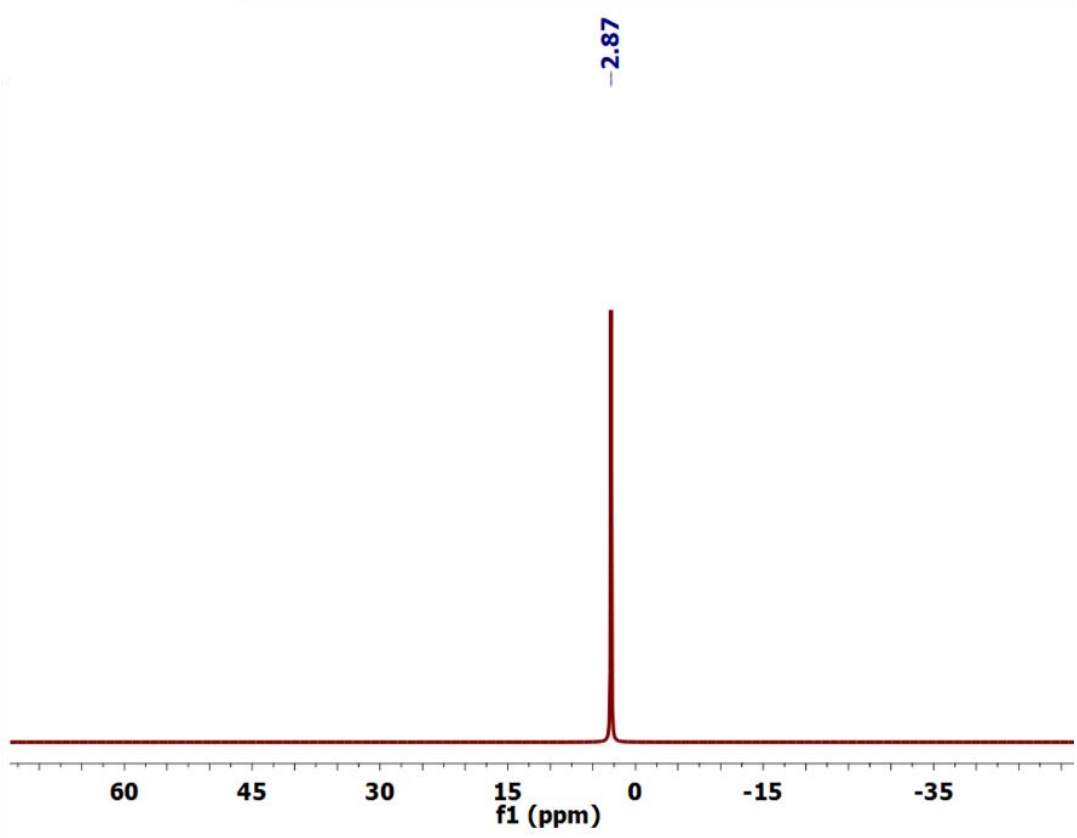

Fig. S10 ^{31}P NMR spectrum in $CDCl_3$ of the Cu_{18} NC.

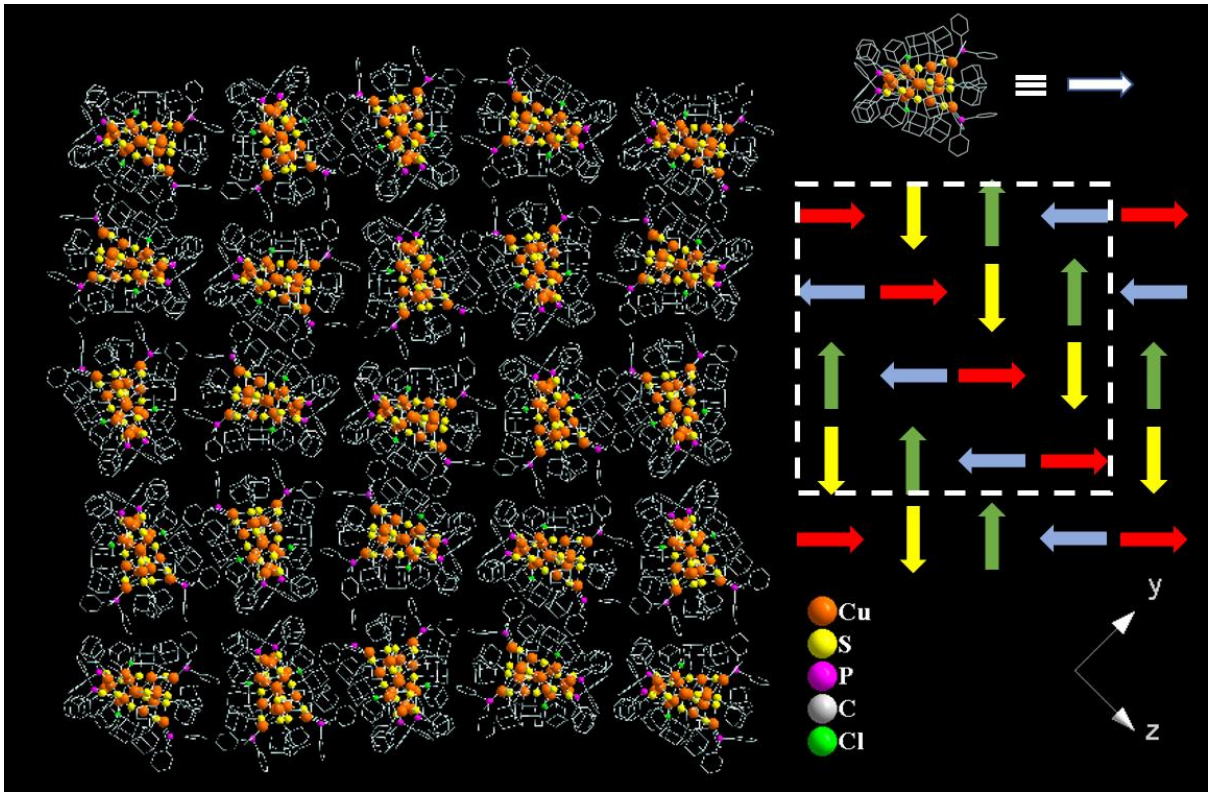

Fig. S11 The herringbone pattern of the Cu_{18} NC caused by the hydrophobic interactions between the adamantane moieties along the *x*-axis.

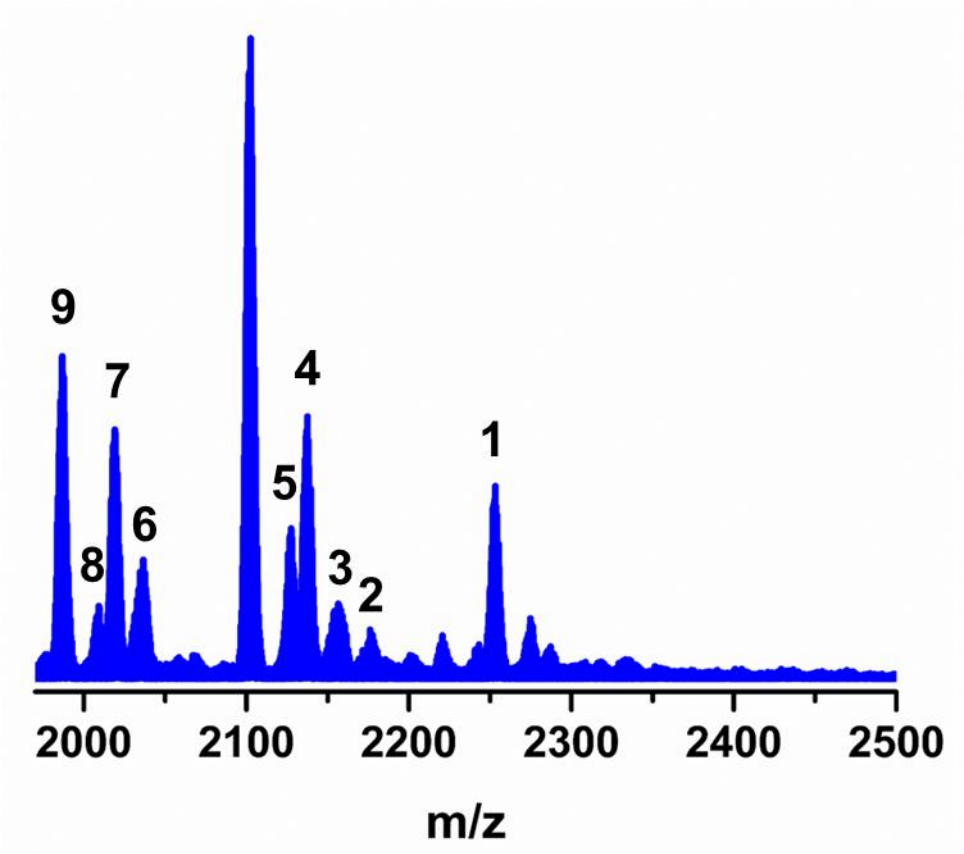

Fig. S12 Partial positive-mode ESI-MS spectrum of the Cu_{18} NC over the range of m/z 1900 to 2500. The numbers show experimental peaks of the corresponding fragments.

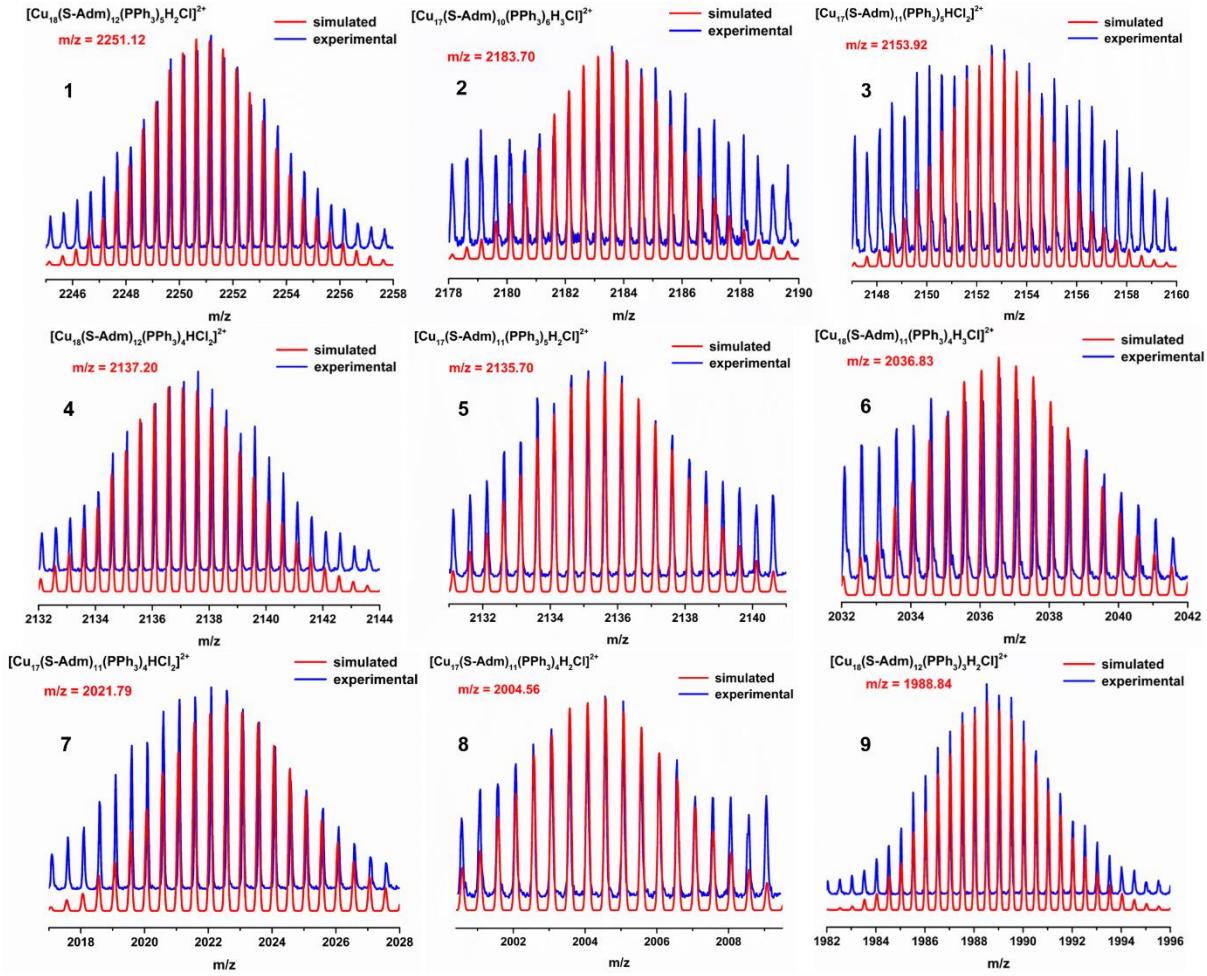

Fig. S13 The numbers show each experimental peaks and their simulated isotopic patterns corresponding to each fragment with a +2 charge.

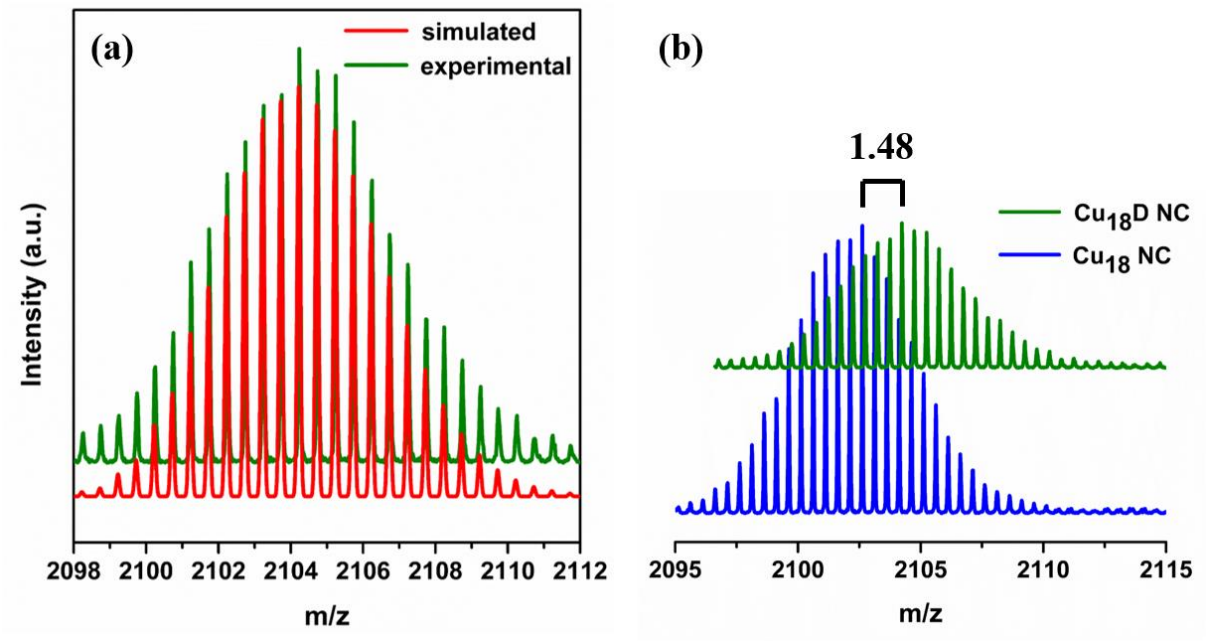

Fig. S14 (a) Experimental and simulated isotopic patterns of the peak corresponding to $[Cu_{18}(S\text{-}Adm)_{12}(PPh_3)_4D_3]^{2+}$, and (b) peak shifting from Cu_{18} NC to Cu_{18}D NC.

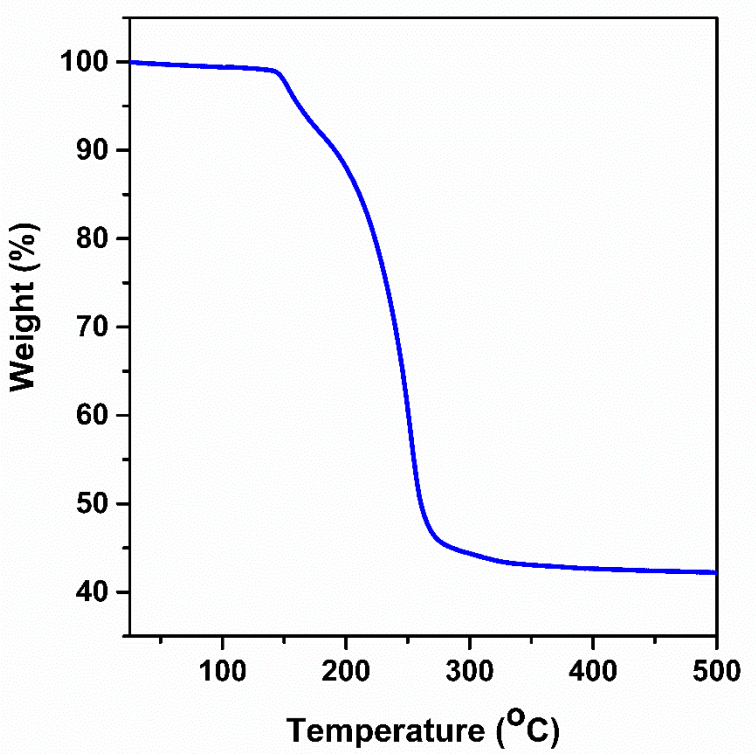

Fig. S15 Thermogravimetric ananlysis of the Cu_{18} NC.

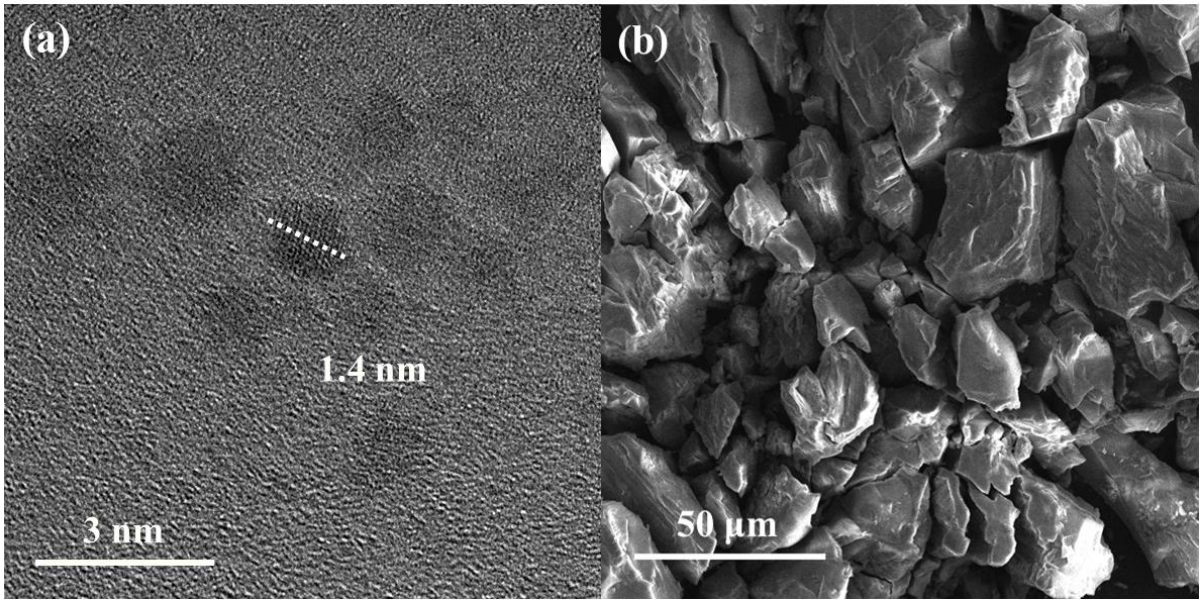

Fig. S16 (a) HR-TEM image, and (b) SEM micrograph of the Cu_{18} NC crystal.

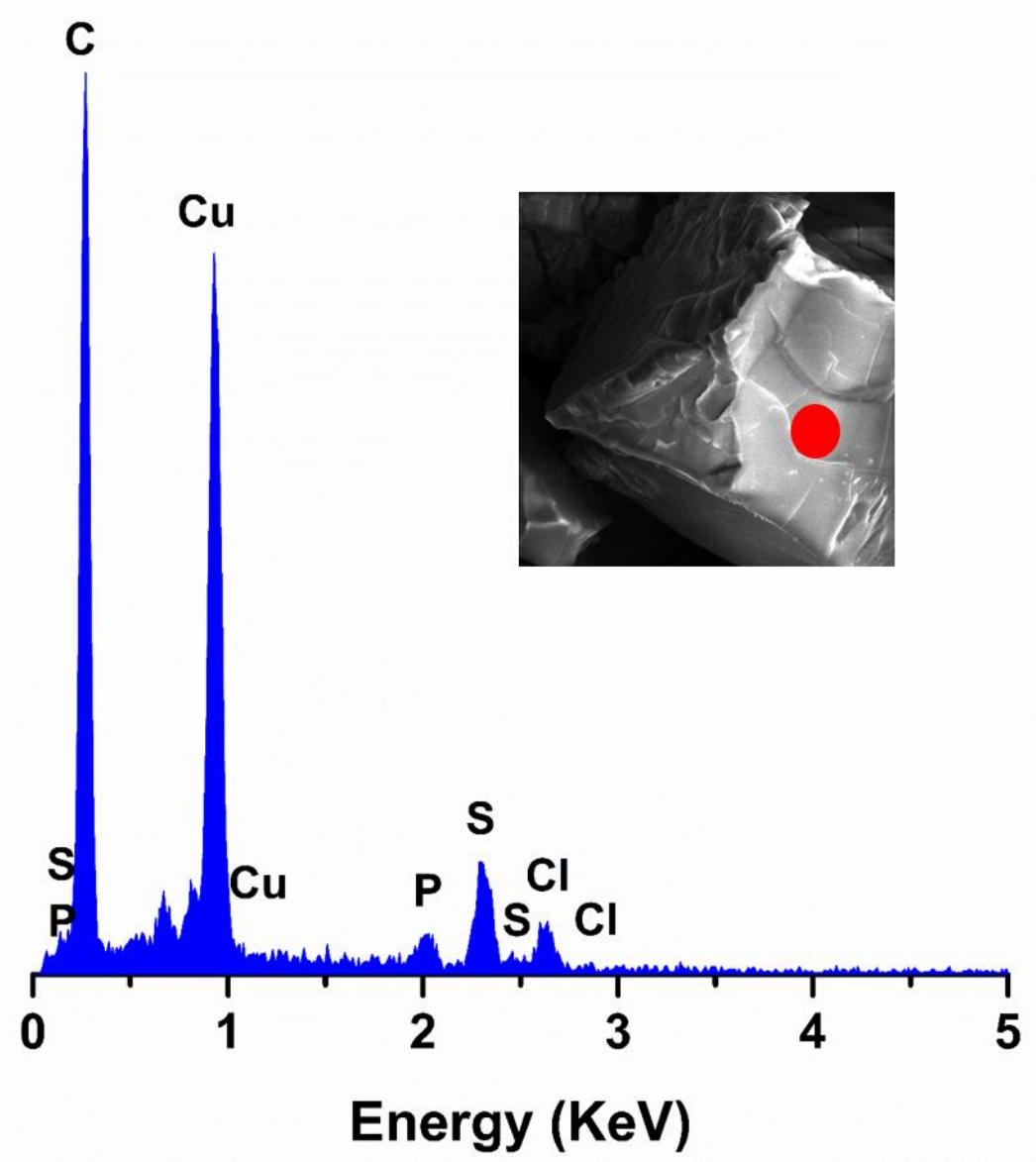

Fig. S17 EDS analysis illustrates the presence of Cu, S, P, Cl, and C as elements in this Cu_{18} NC.

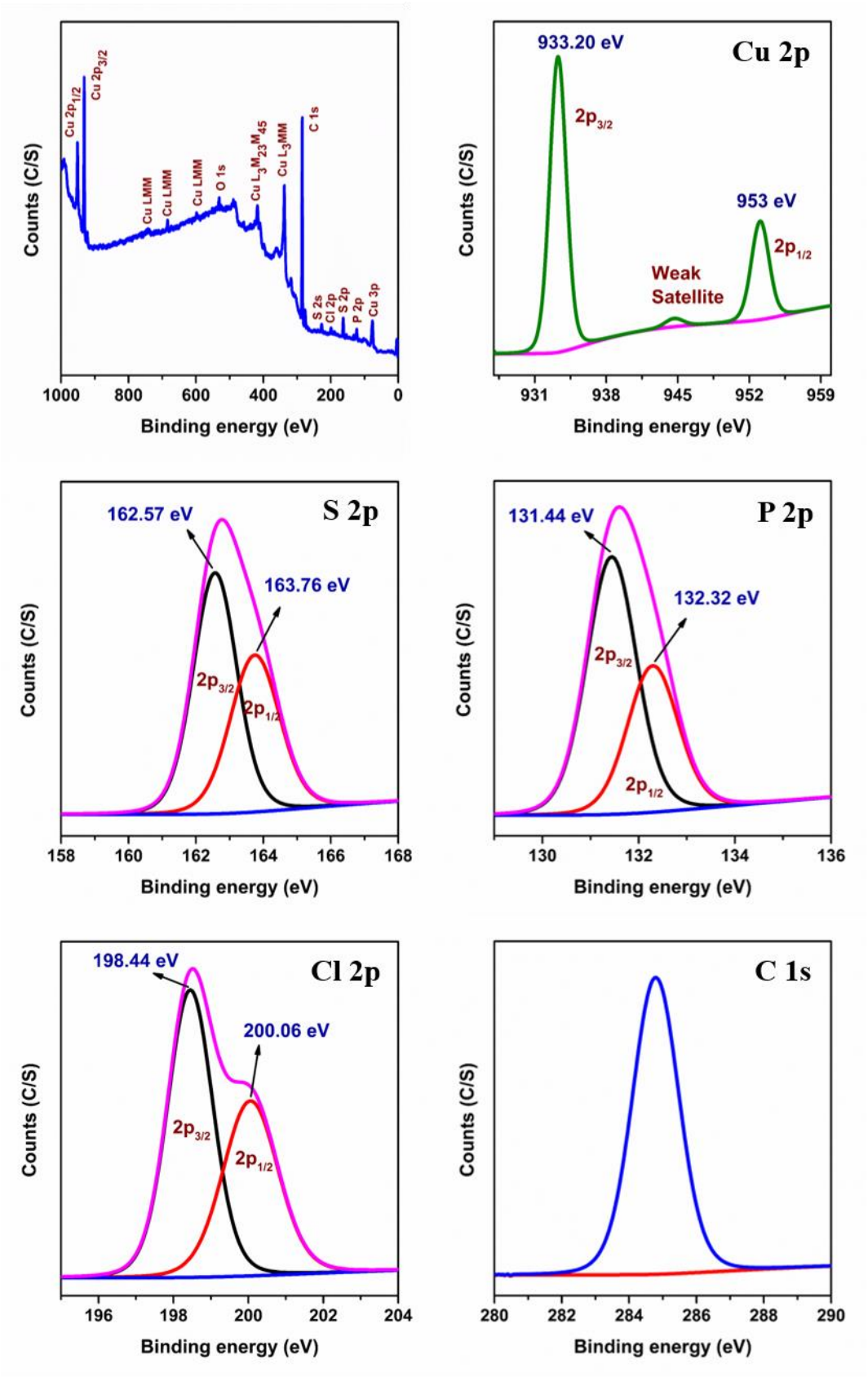

Fig. S18 Survey spectrum and deconvoluted XPS spectra of each element of the Cu_{18} NC.

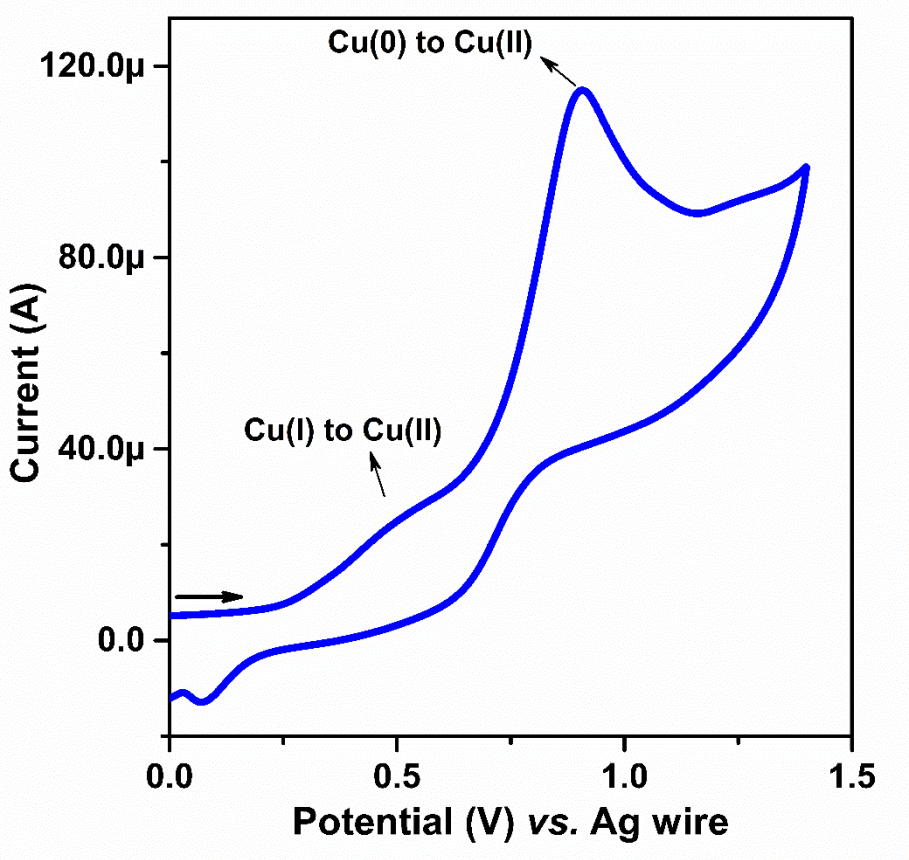

Fig. S19 Cyclic voltammogram data of the Cu_{18} NC.

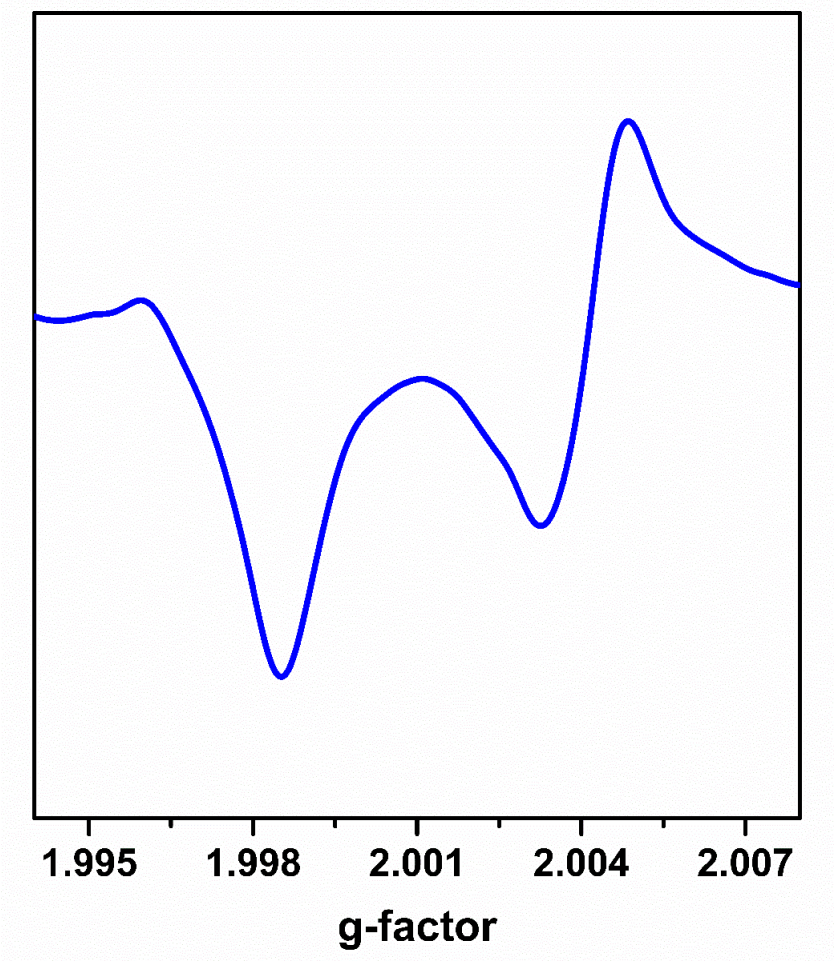

Fig. S20 EPR spectrum of the Cu_{18} NC with respect to g-factor.

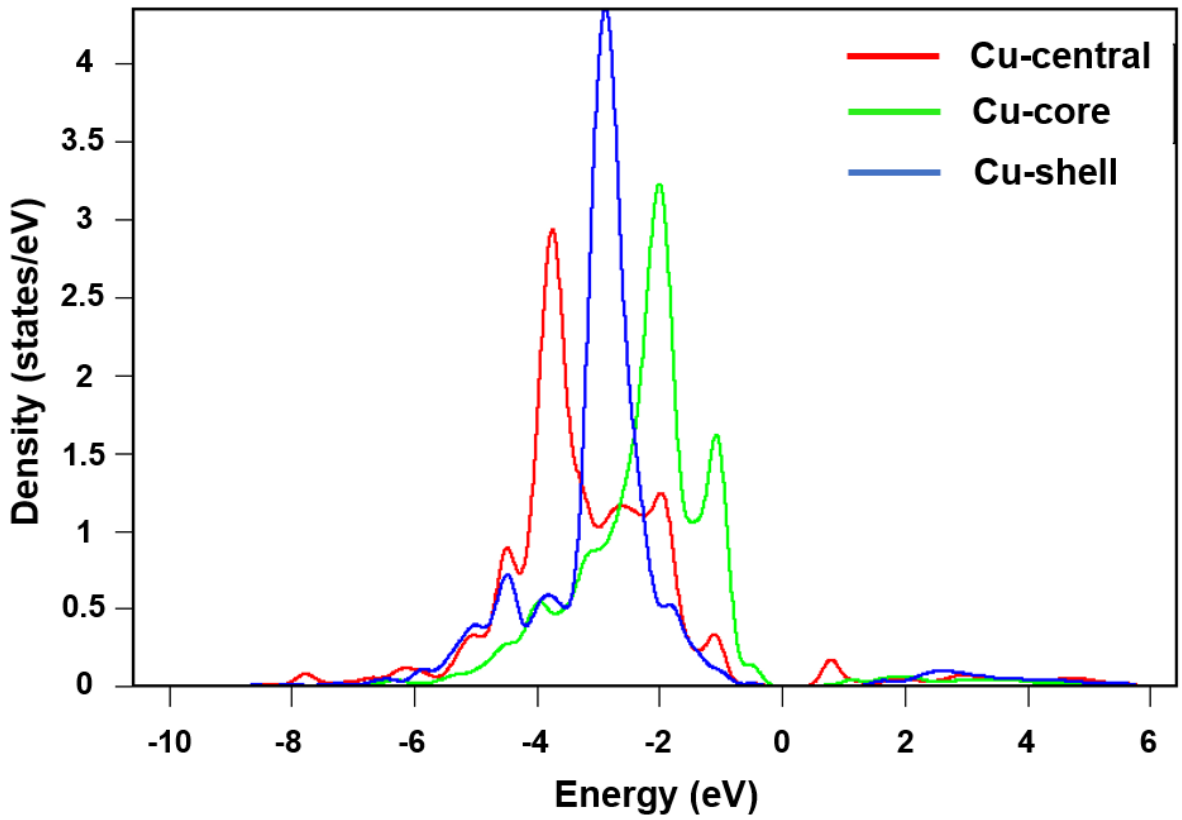

Fig. S21 Localized density of states (LDOS) of different types of Cu atoms in the Cu_{18} NC. Representative atoms from each category are analysed.

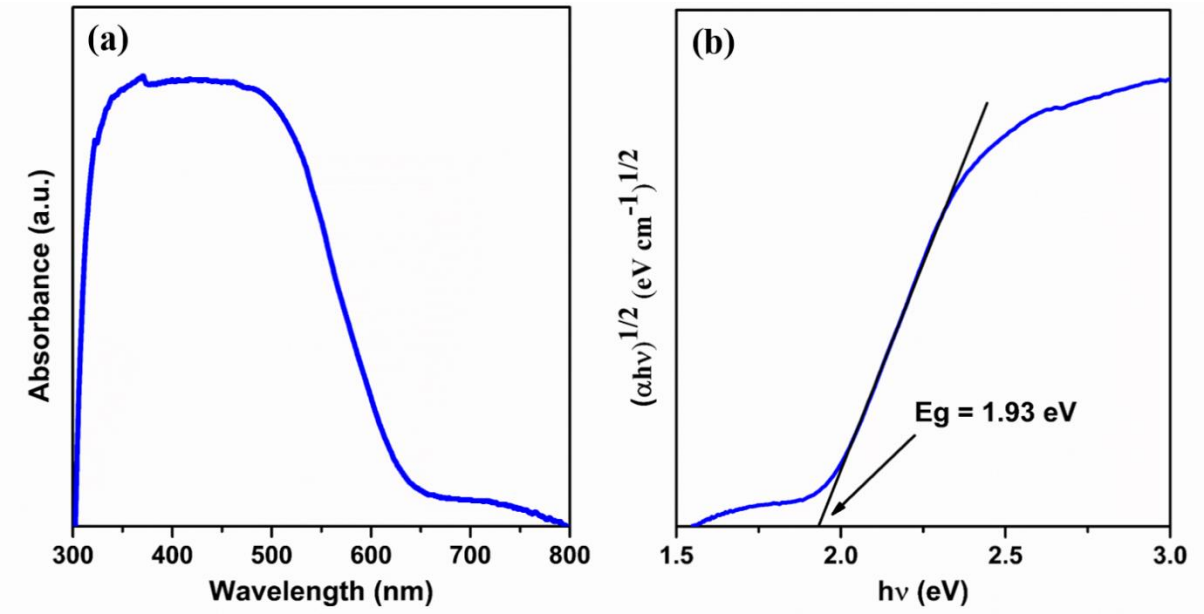

Fig. S22 (a) Solid-state UV-vis absorbance spectrum of the Cu_{18} NC and (b) its characteristic bandgap.

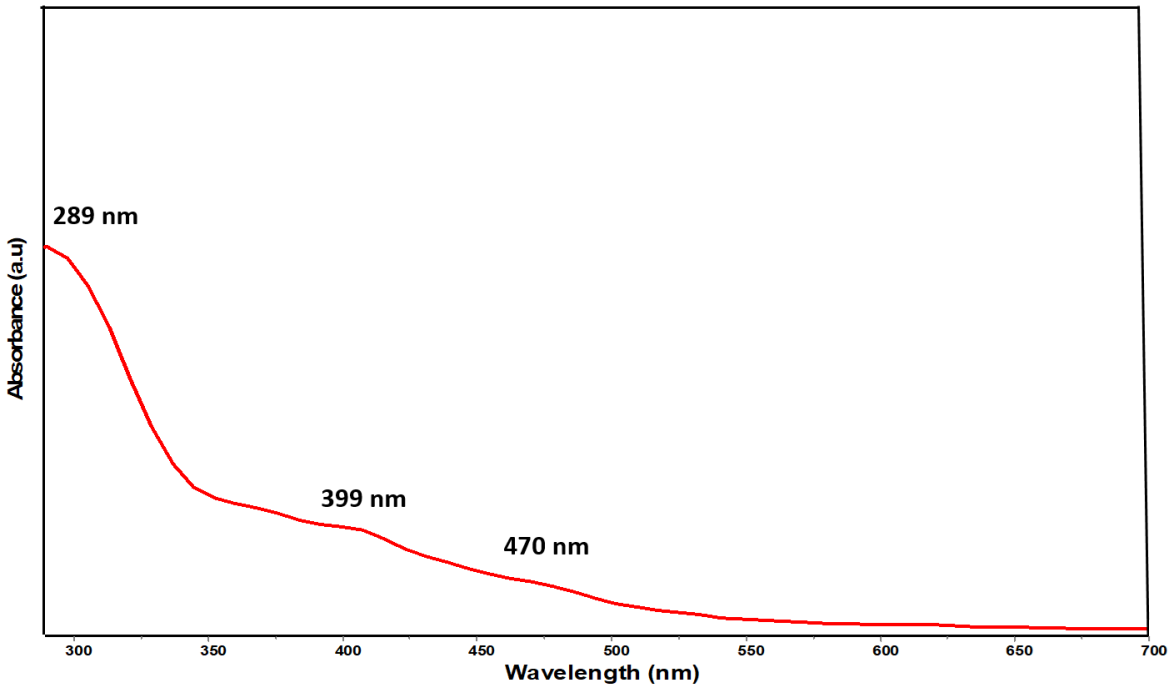

Fig. S23 Simulated absorbance spectrum of the Cu_{18} NC in chloroform.

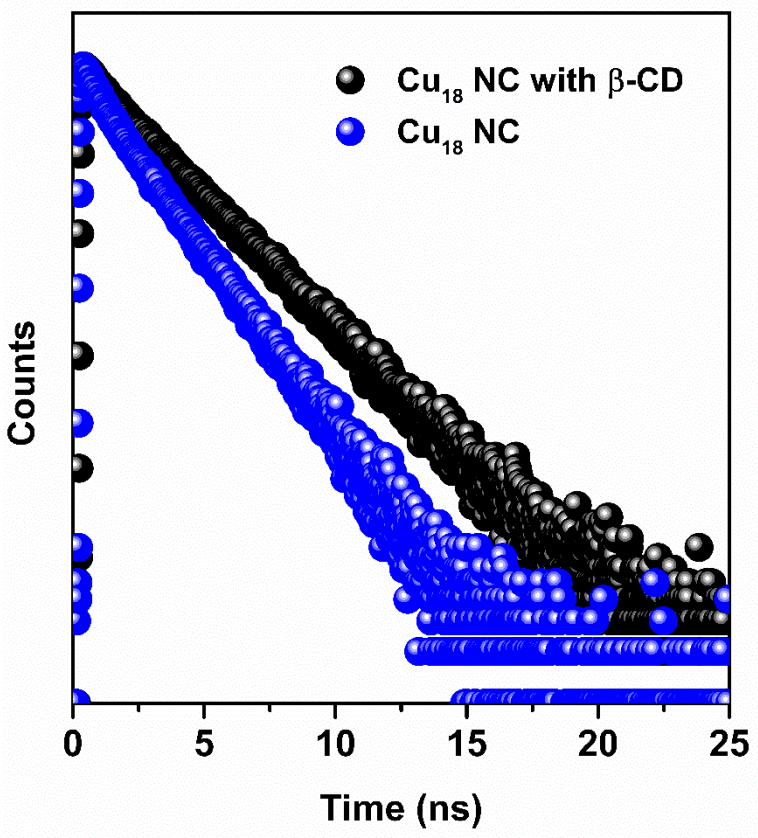

Fig. S24 Emission lifetime of Cu_{18} NC and Cu_{18} NC with β-CD in chloroform medium upon excitation with a 375 nm laser.

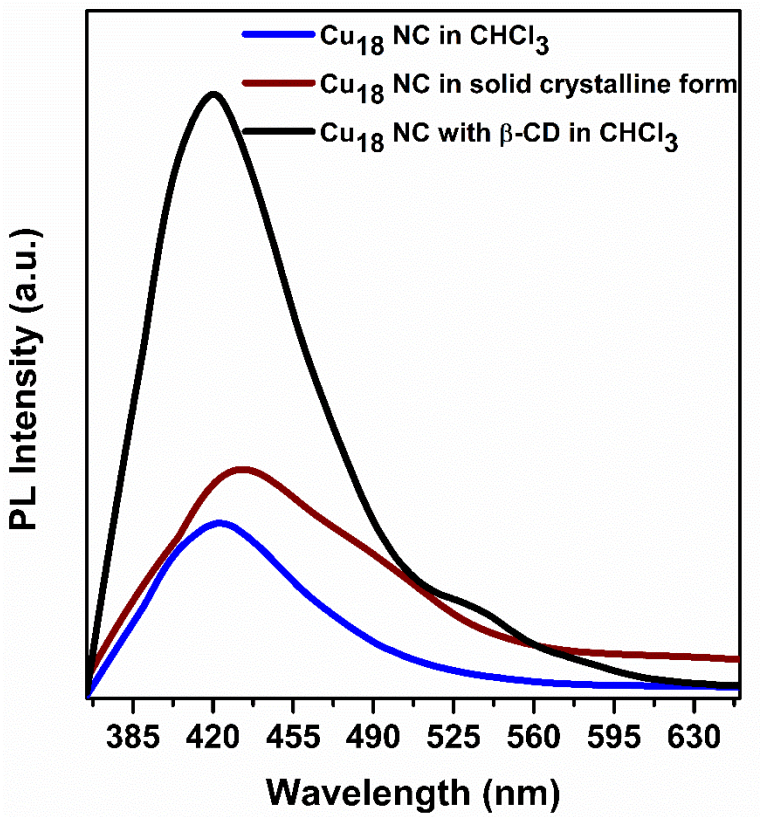

Fig. S25 Difference in PL properties of solid and solution state of Cu_{18} NC and Cu_{18} NC with β-CD.

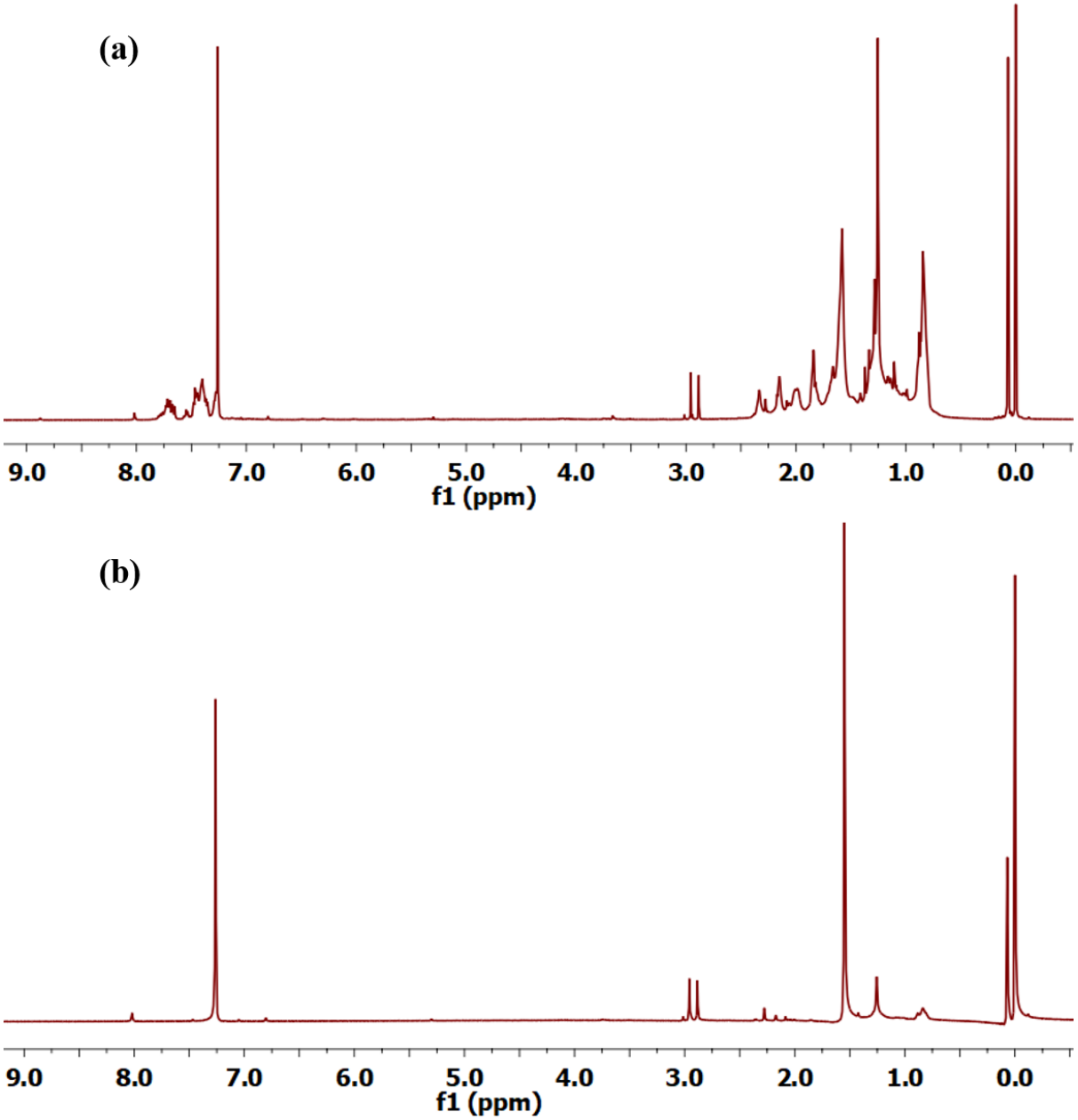

Fig. S26 ^{1}H NMR spectra in $CDCl_3$ of (a) β-CD attached Cu_{18} NC, and (b) pure β-CD.

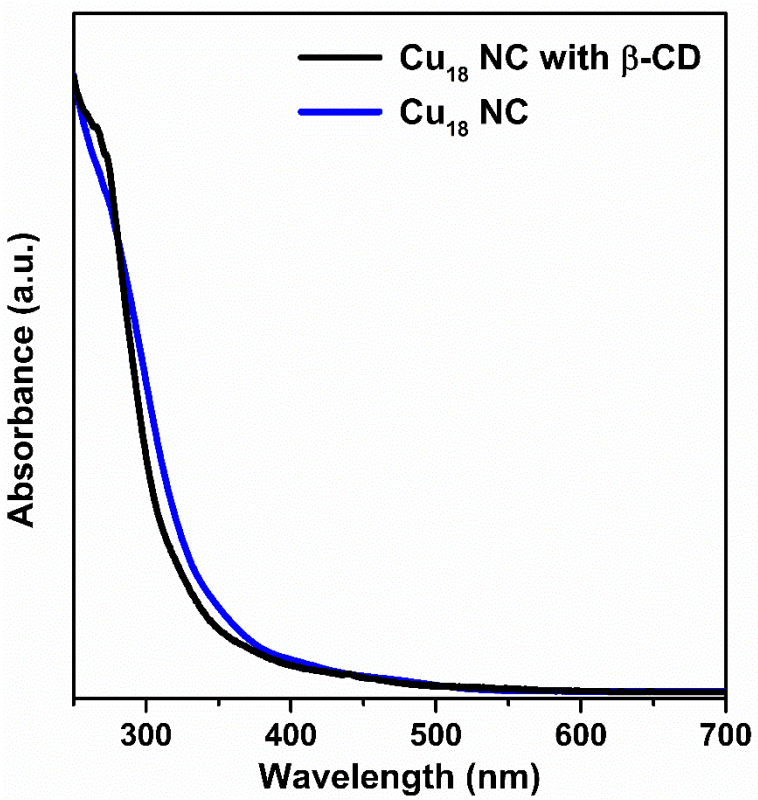

Fig. S27 UV-vis absorbance spectra of the Cu_{18} NC and Cu_{18} NC with β-CD.

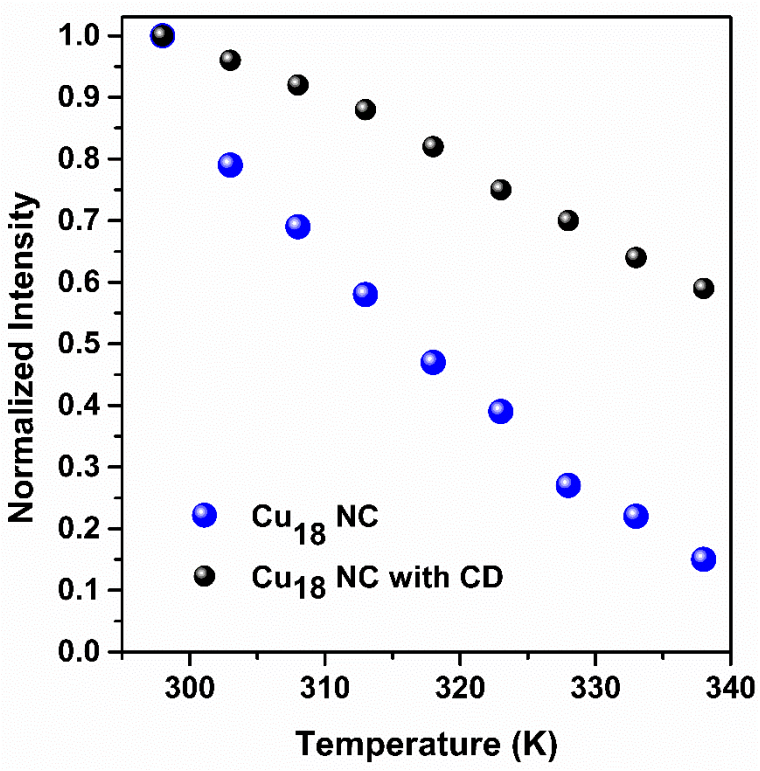

Fig. S28 Temperature-dependent PL property of the Cu_{18} NC and Cu_{18} NC with β-CD.

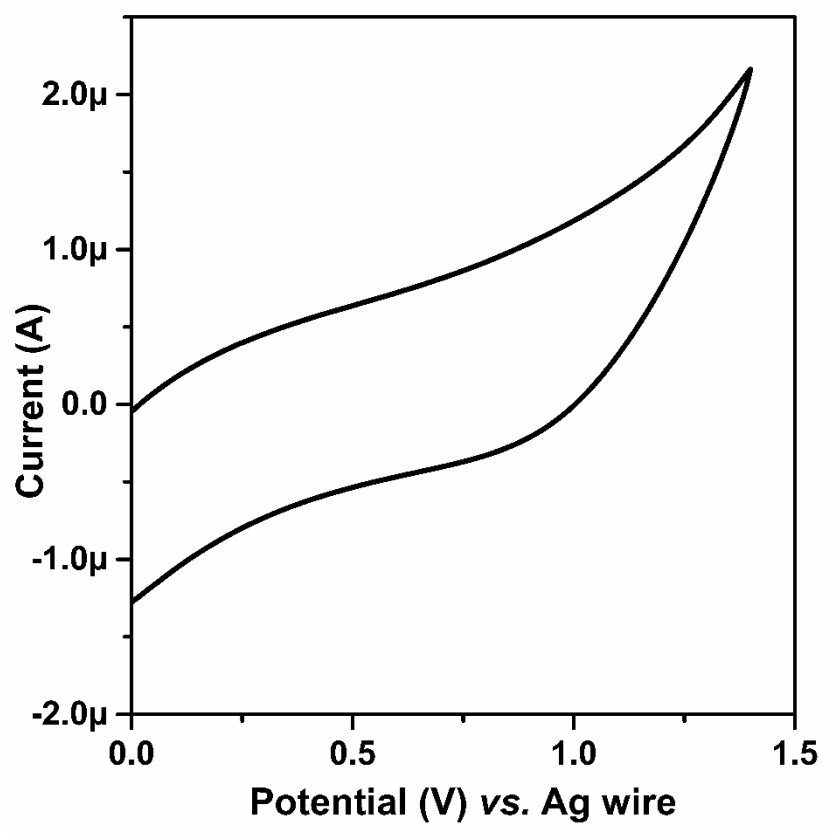

Fig. S29 Cyclic voltammogram data of Cu_{18} NC with β-CD.

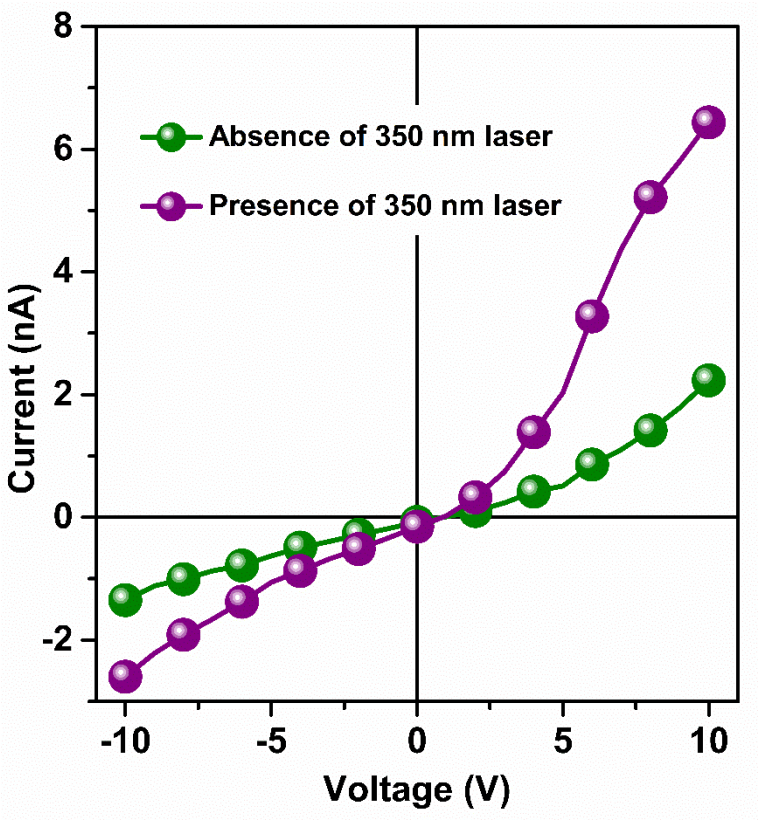

Fig. S30 I-V characteristic plot of the Cu_{18} NC.

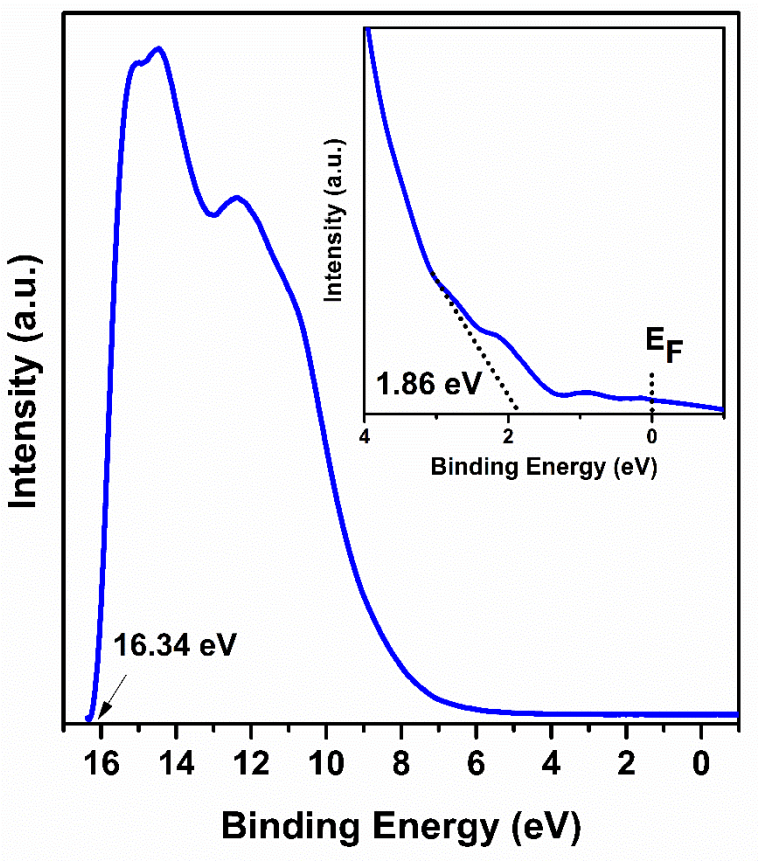

Fig. S31 UPS data of the Cu_{18} NC.

References

S1. S. Lee, M. S. Bootharaju, G. Deng, S. Malola, W. Baek, H. Hakkinen, N. Zheng and T. Hyeon, *J. Am. Chem. Soc.*, 2020, **142**, 13974-13981.

S2. C. Sun, N. Mammen, S. Kaappa, P. Yuan, G. Deng, C. Zhao, J. Yan, S. Malola, K. Honkala, H. Häkkinen, B. K. Teo and N. Zheng, *ACS nano*, 2019, **13**, 5975-5986.

S3. A. Ghosh, R.-W. Huang, B. Alamer, E. Abou-Hamad, M. N. Hedhili, O. F. Mohammed and O. M. Bakr, *ACS Mater. Lett.*, 2019, **1**, 297-302.

S4. S. Nematulloev, R. W. Huang, J. Yin, A. Shkurenko, C. Dong, A. Ghosh, B. Alamer, R. Naphade, M. N. Hedhili, P. Maity, E. Mohammed, O. F. Mohammed and O. M. Bakr, *Small*, 2021, **27,** 2006839.

S5. C. Dong, R.-W. Huang, C. Chen, J. Chen, S. Nematulloev, X. Guo, A. Ghosh, B. Alamer, M. N. Hedhili, T. T. Isimjan, Y. Han, O. F. Mohammed and O. M. Bakr, *J. Am. Chem. Soc.*, 2021, **143**, 11026-11035.

S6. R.-W. Huang, J. Yin, C. Dong, A. Ghosh, M. J. Alhilaly, X. Dong, M. N. Hedhili, E. Abou-Hamad, B. Alamer, S. Nematulloev, Y. Han, O. F. Mohammed and O. M. Bakr, *J. Am. Chem. Soc.*, 2020, **142**, 8696-8705.

S7. Rigaku Oxford Diffraction. CrysAlisPro Software system, version 1.171.40.25a, Rigaku Corporation. Oxford, UK, 2018.

S8. L. Palatinus and G. Chapuis, *J. Appl. Crystallogr.*, 2007, **40,** 786.

S9. G. M. Sheldrick, *Acta Crystallogr., C. Struct. Chem.*, 2015, **71,** 3-8.

S10. O. V. Dolomanov, L. J. Bourhis, R. J. Gildea, J. A. K. Howard and H. J. Puschmann, *Appl. Crystallogr.*, 2009, **42,** 339.

S11. M. J. Frisch, *et al.* Gaussian 09, Revision D.01; Gaussian, Inc. Wallingford, CT, 2009.

S12. A. D. Becke, *J. Chem. Phys.*, 1993, **98,** 5648-5652.

S13. A. D. McLean and G. S. Chandler, *J. Chem. Phys.*, 1980, **72,** 5639 −5648.

S14. P. J. Hay and W. R. Wadt, *J. Chem. Phys.*, 1985, **82,** 270 −283.

S15. P. J. Hay and W. R. Wadt, *J. Chem. Phys.*, 1985, **82,** 299 −310.

S16. T. Lu and F. Chen, *J. Comput. Chem.*, 2012, **33,** 580-592.

S17. T. Lu and F. Chen, *Acta Chim. Sinica*, 2011, **69,** 2393-2406.

S18. K. Wolinski, J. F. Hinton and P. Pulay, *J. Am. Chem. Soc.*, 1990, **112,** 8251−8260.

S19. G. Kresse and J. Hafner. *Phys. Rev. B. Condens. Matter Mater. Phys.*, 1994, **49,** 14251.

S20. J. P. Perdew, J. A. Chevary, S. H. Vosko, K. A. Jackson, M. R. Pederson, D. J. Singh and C. Fiolhais, *Phys. Rev. B. Condens. Matter Mater. Phys.*, 1992, **46,** 6671.

S21. G. Kresse and D. Joubert, *Phys. Rev. B. Condens. Matter Mater. Phys.*, 1999, **59,** 1758.

S22. W. Tang, E. Sanville and G. Henkelman, *J. Phys., Compute Mater.*, 2009, **21**, 084204.